

# Site-Resolved Determination of Peptide Torsion Angle $\phi$ from the Relative Orientations of Backbone N–H and C–H Bonds by Solid-State NMR

M. Hong, J. D. Gross, and R. G. Griffin\*

Francis Bitter Magnet Laboratory and Department of Chemistry, Massachusetts Institute of Technology, Cambridge, Massachusetts 02139

Received: March 10, 1997; In Final Form: May 12, 1997<sup>⊗</sup>

We describe a method for determining the torsion angle  $\phi$  in peptides. The technique is based on the measurement of the relative orientation of the N–H<sup>N</sup> and C <sup>$\alpha$</sup> –H <sup>$\alpha$</sup>  bonds, which is manifested in the rotational sideband spectrum of the sum and difference of the two corresponding dipolar couplings. The method exploits <sup>15</sup>N–<sup>13</sup>C double-quantum and zero-quantum coherences, which evolve simultaneously under the N–H and C–H dipolar interactions. The magnitudes of these dipolar couplings scaled by the proton homonuclear decoupling sequence are directly extracted from control experiments that correlate the dipolar interactions with the isotropic chemical shifts. Applied to <sup>15</sup>N-labeled *N*-acetyl-D,L-valine, the experiment yielded  $\phi = -135^\circ$ , which agrees well with the X-ray crystal structure. Simulations indicate that the accuracy of the measured angle  $\phi$  is within  $\pm 10^\circ$  when the N–H<sup>N</sup> and C <sup>$\alpha$</sup> –H <sup>$\alpha$</sup>  bonds are approximately antiparallel and  $\pm 20^\circ$  when they are roughly parallel. The technique is sufficiently sensitive to be applied to small peptides that are only labeled in <sup>15</sup>N and to larger polypeptides that are uniformly and randomly labeled in both <sup>15</sup>N and <sup>13</sup>C. It allows  $\phi$  angles in various residues to be measured simultaneously and resolved by the C <sup>$\alpha$</sup>  chemical shifts.

## 1. Introduction

The study of the three-dimensional structures of biomolecules in the solid state by nuclear magnetic resonance (NMR) spectroscopy has relied primarily on the measurement of internuclear distances through dipolar couplings. In order to resolve different chemical moieties in the NMR spectra, these distance measurements generally require magic-angle spinning (MAS) or macroscopically oriented samples. In the limit  $\omega_r \gg |H_D|$ , where  $\omega_r$  is the spinning speed and  $|H_D|$  is the size of the dipolar Hamiltonian, the anisotropic dipolar interactions are efficiently attenuated unless specific radio frequency (rf) pulses or spinning speeds are used to interfere with rotational averaging and thus “recouple” the spins of interest. Accordingly, a number of homonuclear<sup>1–5</sup> and heteronuclear<sup>6–8</sup> dipolar recoupling techniques have been proposed to selectively recouple the dipolar interaction of an isolated spin pair. However, efforts in achieving broad-band dipolar recoupling, which is crucial for obtaining multiple distances simultaneously, have met significant challenges because weak, long-range dipolar interactions containing the distance parameters of interest are masked by strong, short-range couplings.<sup>5,9</sup>

Alternatively, biomolecular structures may be studied through the measurement of torsion angles, which constrain molecular conformations via the relative orientations of adjacent segments. For example, the secondary structures of proteins are characterized by backbone torsion angles  $\phi$  and  $\psi$ , which can be mapped in a Ramachandran plot.<sup>10</sup> For molecules undergoing fast isotropic motions in solutions, torsion angles can be determined from three-bond scalar couplings using the empirical Karplus equations.<sup>11,12</sup> For rigid and semirigid solids, in which anisotropic spin interactions are not averaged by motion, torsion angles can be extracted by correlating the orientations of two segment-fixed NMR interaction tensors, such as the chemical shift and the dipolar coupling, across the torsional bond.

This approach to determining molecular structures in the solid state has recently been pursued in several laboratories.<sup>13–17</sup> For

example, by correlating two C–H dipolar couplings across a C–C bond, the *cis* and *trans* conformations of a H–C=C–H moiety in two aliphatic dicarboxylates were distinguished.<sup>13</sup> Also, by correlating the chemical shift anisotropy of the carbonyl carbon with the C–H coupling of the neighboring  $\alpha$  carbon in an amino acid, the angle  $\psi$  was determined.<sup>14</sup> These experiments have been carried out under either static or MAS conditions. However, to obtain torsion angles in large biomolecules, the required spectral sensitivity and site resolution, which is prerequisite for extracting multiple torsion angles at once, make MAS the method of choice. A relatively common feature in the torsion angle techniques developed so far is the incorporation of two <sup>13</sup>C labels to enhance the spectral sensitivity and to create <sup>13</sup>C double-quantum coherence. Double-quantum coherence not only allows the two NMR interaction frequencies to be measured concurrently but also suppresses signals of isolated spins, thus simplifying the spectra. However, it is worth mentioning that the torsion angle  $\psi$  in an amino acid has also been determined successfully without double-quantum coherence.<sup>18</sup>

To determine a torsion angle from the relative orientations of two NMR tensors, the orientation of each tensor in a common reference frame must be known. While the dipolar interaction tensor has a well-defined cylindrical symmetry (i.e. an asymmetry parameter  $\eta = 0$ ) with its unique axis along the internuclear vector, the orientation of a chemical shift tensor with respect to the molecular segment is usually not known *a priori* and needs to be measured separately. Therefore, it is simpler to measure the torsion angle via the orientations of two dipolar coupling tensors across the intervening bond. For instance, the peptide backbone torsion  $\phi = \text{C}(\text{O})\text{--N--C}^\alpha\text{--C}(\text{O})$  can be obtained from the relative orientations of the N–H<sup>N</sup> and C <sup>$\alpha$</sup> –H <sup>$\alpha$</sup>  dipolar tensors, whose unique axes are along the respective bonds. The corresponding torsion angle H<sup>N</sup>–N–C <sup>$\alpha$</sup> –H <sup>$\alpha$</sup> , termed  $\phi_H$  in the following, is directly related to  $\phi$  according to  $\phi_H = \phi - 60^\circ$  for the commonly occurring L-amino acids and  $\phi_H = \phi + 60^\circ$  for D-amino acids. The relation

<sup>⊗</sup> Abstract published in *Advance ACS Abstracts*, July 1, 1997.

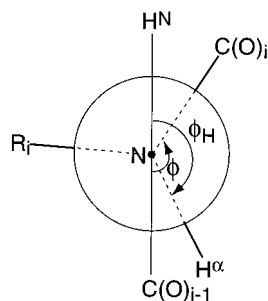


**Figure 1.** Newman projection of a L-amino acid, viewed from the N–C $\alpha$  vector into the plane of the paper. The backbone torsion angle  $\phi$  is defined as C(O) $_{i-1}$ –N–C $\alpha$ –C(O) $_i$ , where  $i$  is the residue (R) number, and is negative as drawn here. The corresponding NMR-measurable  $\phi_H$  (H $^N$ –N–C $\alpha$ –H $^\alpha$ ) is related to  $\phi$  by  $\phi_H = \phi - 60^\circ$  for L-amino acids. The trans conformation corresponds to  $\phi_H = 180^\circ$ , while the cis conformation corresponds to  $0^\circ$ .

between  $\phi$  and  $\phi_H$  is illustrated in a Newman projection of a peptide residue linkage in Figure 1.

In this paper, we demonstrate the measurement of  $\phi$  in  $^{15}\text{N}$ -labeled *N*-acetyl-D,L-valine (NAV) by a two-dimensional (2D) MAS technique that correlates the C $\alpha$ –H $\alpha$  and N–H $^N$  bond orientations. The technique is a variation of the H–C=C–H experiment,<sup>13</sup> but involves the evolution of heteronuclear ( $^{15}\text{N}$ – $^{13}\text{C}$ ) double- and zero-quantum coherences instead of the homonuclear ( $^{13}\text{C}$ – $^{13}\text{C}$ ) double-quantum coherence. In accordance with the convention in solution-state NMR spectroscopy, we refer to this combination of  $^{15}\text{N}$ – $^{13}\text{C}$  double- and zero-quantum coherences as heteronuclear multiple-quantum coherences.<sup>19–21</sup> We show that the N–C dipolar interaction can be recoupled under MAS with high efficiency, so that sensitive NMR spectra can be obtained even for this natural abundance  $^{13}\text{C}$  sample. The one-bond C–H and N–H couplings, which are input parameters for the simulations of the  $\phi$ -dependent heteronuclear multiple-quantum (HMQ) spectra, can be directly determined by single-quantum  $^{13}\text{C}$  and  $^{15}\text{N}$  dipolar-shift correlation experiments. Most importantly, the technique yields  $\phi$  angles in a site-resolved fashion, thus making it possible to determine multiple  $\phi$  angles simultaneously in conveniently labeled peptides and proteins.

## 2. Experimental Section

All experiments were performed on a custom-designed spectrometer operating at 397.8 MHz for  $^1\text{H}$ , 100.0 MHz for  $^{13}\text{C}$ , and 40.3 MHz for  $^{15}\text{N}$  nuclei. A custom-designed triple-resonance transmission-line probe with a 4 mm Chemagnetics (Fort Collins, CO) MAS spinning module was used. The transmission-line design enables high rf powers to be used on all three channels without arcing. Proton rf fields of about 100 kHz were used for excitation and CW decoupling. The  $^1\text{H}$   $90^\circ$  pulse length for MREV-8 multiple-pulse decoupling was 3  $\mu\text{s}$ . During the evolution period, the semiwindowless version of MREV-8 was employed and incremented in half-cycles, typically 18  $\mu\text{s}$ , in order to increase the spectral width of the indirect dimension.  $^{13}\text{C}$  and  $^{15}\text{N}$   $90^\circ$  pulse lengths were 4 and 6.2  $\mu\text{s}$ , respectively. The spinning speeds were controlled to  $\pm 2$  Hz by a Doty (Columbia, SC) spinning speed controller. For the torsion angle and the  $^{13}\text{C}$  DIPSHIFT experiments,  $\omega_r/2\pi = 2525$  Hz, while for the  $^{15}\text{N}$  DIPSHIFT measurement,  $\omega_r/2\pi = 2137$  Hz. The HMQ excitation and reconversion times corresponded to two rotor periods and were not further optimized by varying the spinning speed. The recycle delay was 2.5 s in all experiments. The cross polarization contact time was 2 ms.

Uniformly  $^{15}\text{N}$ -labeled *N*-acetyl-D,L-valine in powder form was purchased from Cambridge Isotope Laboratories, Inc. (Andover, MA), and was recrystallized from aqueous solution

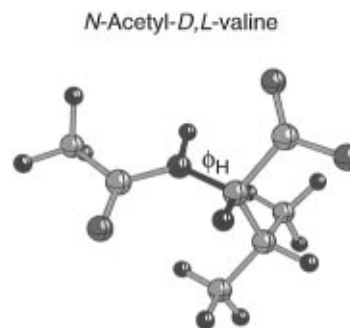


**Figure 2.** X-ray crystal structure of *N*-acetyl-D,L-valine, obtained from ref 35. The C(O)–N–C $\alpha$ –C(O) torsion angle was determined to be  $-136.5^\circ$ .

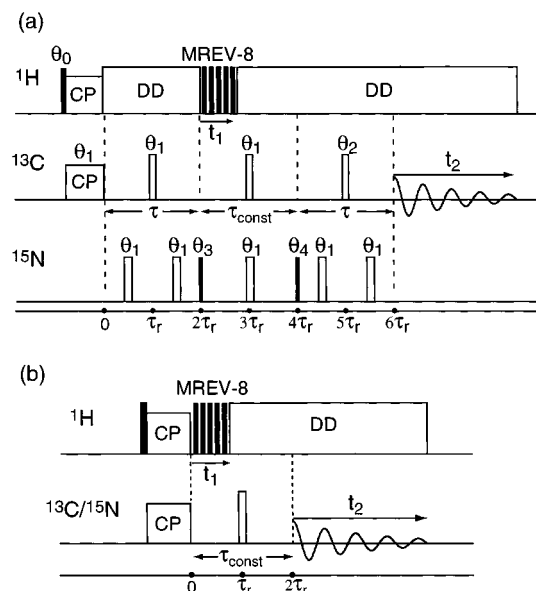


**Figure 3.** (a) Pulse sequence for obtaining  $^{15}\text{N}$ – $^{13}\text{C}$  HMQ dipolar sideband spectra. The N–C dipolar interaction is recoupled under MAS by rotor-synchronized  $^{15}\text{N}$  and  $^{13}\text{C}$   $180^\circ$  pulses during  $\tau$ . The excited N–C double- and zero-quantum coherences evolve during  $t_1$  under C–H and N–H dipolar interactions, with  $^1\text{H}$  homonuclear couplings removed by MREV-8 multiple-pulse decoupling. The evolution period has a maximum length of one rotor period, which is half of the constant time  $\tau_{\text{const}}$ . A  $^{13}\text{C}$  and a  $^{15}\text{N}$   $180^\circ$  pulse are applied in the middle of  $\tau_{\text{const}}$  to refocus  $^{13}\text{C}$  and  $^{15}\text{N}$  isotropic chemical shifts, respectively. The N–C HMQ coherences are then reconverted to single-quantum  $^{13}\text{C}$  coherence for the detection of  $^{13}\text{C}$  chemical shift during  $t_2$ . The phase cycle is  $\theta_0 = 13$ ,  $\theta_1 = 11223344$ ,  $\theta_2 = 22334411$ ,  $\theta_3 = 24134231$ ,  $\theta_4 = 22114433$ , receiver = 11223344, where the indices 1, 2, 3, 4 correspond to four orthogonal phases  $x$ ,  $y$ ,  $-x$ ,  $-y$ , respectively. (b) DIPSHIFT pulse sequence for measuring C–H and N–H dipolar couplings separated by the  $^{13}\text{C}$  and  $^{15}\text{N}$  chemical shifts, respectively. The evolution period is similar to that of the previous experiment in order to extract the C–H and N–H couplings to be used in the simulation of the  $\phi$ -dependent HMQ spectra.

to reduce chemical shift dispersion due to conformational heterogeneity. The resulting C $\alpha$  line widths in the MAS spectra were about 0.6 ppm. The X-ray crystal structure of NAV is shown in Figure 2.

## 3. Theory for Correlating N–H $^N$ and C $\alpha$ –H $\alpha$ Tensor Orientations

The pulse sequence for determining the H $^N$ –N–C $\alpha$ –H $\alpha$  torsion angle under MAS is shown in Figure 3a. First, transverse  $^{13}\text{C}$  magnetization is created by cross polarization from  $^1\text{H}$  and evolves under the influence of the recoupled  $^{15}\text{N}$ – $^{13}\text{C}$  dipolar interaction for a period  $\tau$ . The N–C dipolar recoupling is achieved by rotor-synchronized  $^{15}\text{N}$  and  $^{13}\text{C}$   $180^\circ$

pulses, with the  $^{15}\text{N}$  pulses at the center and the  $^{13}\text{C}$  pulses at the end of each rotor cycle.<sup>6,22,23</sup> These  $180^\circ$  pulses perturb rotational averaging of the anisotropic dipolar interaction so that antiphase magnetization  $C_y N_z$ , where  $C$  and  $N$  refer to  $^{13}\text{C}$  and  $^{15}\text{N}$  spins, respectively, is created. A  $^{15}\text{N}$   $90^\circ$  pulse converts  $C_y N_z$  into a combination of double- and zero-quantum coherences,  $C_y N_x$ . Next, a semiwindowless MREV-8 pulse train is applied on the  $^1\text{H}$  channel to attenuate the homonuclear  $^1\text{H}$  interactions. The MREV-8 sequence is incremented and defines the evolution time  $t_1$ , which has a maximum length of one rotor period. At the end of this rotor period, a pair of  $180^\circ$  pulses are applied on the  $^{15}\text{N}$  and  $^{13}\text{C}$  channels, followed by an additional rotor cycle with continuous proton decoupling. Since the  $180^\circ$  pulses are placed at the center of this constant time period ( $\tau_{\text{const}}$ ),  $^{15}\text{N}$  and  $^{13}\text{C}$  chemical shifts are refocused. In addition, the N–C dipolar couplings are refocused after an integer number of rotor periods by MAS. Thus, the effective Hamiltonian governing the evolution of the N–C multiple-quantum coherences during  $\tau_{\text{const}}$  consists of the C–H and N–H dipolar couplings. Neglecting the long-range couplings, the Hamiltonian is written as

$$\bar{H}(t) = \kappa[\omega_{\text{CH}}(t)2C_z^\alpha H_z^\alpha + \omega_{\text{NH}}(t)2N_z H_z^{\text{NH}}] \quad (1)$$

where the coefficient  $\kappa$  is the scaling factor appropriate to the homonuclear decoupling sequence.

After  $\tau_{\text{const}}$ , a second  $^{15}\text{N}$   $90^\circ$  pulse and N–C recoupling period reconvert the N–C multiple-quantum coherences into observable  $^{13}\text{C}$  magnetization, which is then detected during  $t_2$  under continuous proton decoupling. Double Fourier transformation of the resulting 2D time signal yields N–C multiple-quantum dipolar sideband patterns in the  $\omega_1$  dimension, separated according to the  $^{13}\text{C}$  isotropic chemical shifts in the  $\omega_2$  dimension.

The transformations of the spin density operators under the pulse sequence of Figure 3a are outlined as

$$\begin{aligned} C_x &\xrightarrow{\tau} C_y N_z f(\tau) \xrightarrow{90^\circ_y^{15}\text{N}} C_y N_x f(\tau) \xrightarrow{t_1} \\ &C_y N_x f(\tau) \cos(\Psi_{\text{CH}}(t_1)) \cos(\Psi_{\text{NH}}(t_1)) \xrightarrow{90^\circ_y^{15}\text{N}} \\ &C_y N_z f(\tau) \cos(\Psi_{\text{CH}}(t_1)) \cos(\Psi_{\text{NH}}(t_1)) \xrightarrow{\tau} \\ &-C_x f^2(\tau) \cos(\Psi_{\text{CH}}(t_1)) \cos(\Psi_{\text{NH}}(t_1)) \quad (2) \end{aligned}$$

where only observable magnetization derived from the HMQ coherences is considered. Here,  $\Psi_\lambda(t_1)$  ( $\lambda = \text{CH}, \text{NH}$ ) are the MAS phase angles accumulated during  $t_1$  due to the C–H and N–H dipolar interactions,

$$\Psi_\lambda(t_1) = \int_0^{t_1} dt \omega_\lambda(t) \quad (3)$$

The function  $f(\tau) = \sin(\bar{\omega}_D \tau)$  describes the excitation of the HMQ coherences, where  $\bar{\omega}_D$  is the average N–C coupling under the excitation sequence used here.<sup>24,25</sup> The amplitude modulation  $\cos(\Psi_{\text{CH}}(t_1)) \cos(\Psi_{\text{NH}}(t_1))$  of the observed  $^{13}\text{C}$  magnetization in eq 2 can be rewritten as

$$\cos\left[\frac{\Psi_{\text{CH}}(t_1) + \Psi_{\text{NH}}(t_1)}{2}\right] + \cos\left[\frac{\Psi_{\text{CH}}(t_1) - \Psi_{\text{NH}}(t_1)}{2}\right] \quad (4)$$

We now show that these sum and difference dipolar phases depend on the relative orientations of the two dipolar coupling tensors, whose unique axes are along the  $\text{C}^\alpha\text{--H}^\alpha$  and  $\text{N--H}^{\text{NH}}$  bonds and therefore reflect the torsion angle  $\phi_{\text{H}}$ . The time-dependent dipolar coupling  $\omega_\lambda(t)$  that determines the dynamic phase  $\Psi_\lambda(t_1)$  can be expressed as a Fourier series<sup>25,26</sup>

$$\omega_\lambda(t) = \sum_{m=-2}^2 \omega_\lambda^m(\Omega_{\text{PR}}) e^{im\omega_r t} \quad (5)$$

where  $\omega_\lambda^m(\Omega_{\text{PR}})$  are time-independent frequencies calculated from the following coordinate transformations:

$$\omega_\lambda^m(\Omega_{\text{PR}}) = -\delta_\lambda \left\{ \sum_{m'=-2}^2 D_{0,m'}^{(2)}(\Omega_{\text{PM}}^\lambda) D_{m',-m}^{(2)}(\Omega_{\text{MR}}) \right\} d_{-m,0}^{(2)}(\beta_{\text{RL}}) \quad (6)$$

Here  $\delta_\lambda$  represents the rigid-limit anisotropy of the dipolar interaction  $\lambda$ . The Wigner rotation matrices  $D^{(2)}(\Omega_{\text{PR}}) = D^{(2)}(\Omega_{\text{PM}}) \cdot D^{(2)}(\Omega_{\text{MR}})$  effect coordinate transformations from the principal axis systems of the dipolar coupling tensors to the rotor frame with Euler angles  $\Omega_{\text{PR}} = (\alpha_{\text{PR}}, \beta_{\text{PR}}, \gamma_{\text{PR}})$ .<sup>27</sup> The reduced rotation matrix  $d_{-m,0}^{(2)}(\beta_{\text{RL}})$  dictates the transformation from the rotor frame to the laboratory frame with  $\beta_{\text{RL}} = \tan^{-1}\sqrt{2}$ . The orientations of the  $\text{C}^\alpha\text{--H}^\alpha$  and  $\text{N--H}^{\text{NH}}$  dipolar tensors are expressed in a common molecular frame  $M$ , which is defined such that the relative orientations of the two bonds with respect to the  $Z_M$  axis are easily determined by inspection. Combining eqs 3–6, it can be seen that the sum and difference phases that determine the HMQ spectra are intrinsically the sum and difference frequencies of two segment-fixed dipolar couplings,  $\omega_{\text{CH}}^m(\Omega_{\text{PM}}^{\text{CH}}) \pm \omega_{\text{NH}}^m(\Omega_{\text{PM}}^{\text{NH}})$ , in which the segment-fixed Euler angles  $\Omega_{\text{PM}}$  contain information on the torsion angle  $\phi_{\text{H}}$  or  $\phi$ . The simplest choice of  $Z_M$  corresponds to the N–C bond direction. In this case,  $\gamma_{\text{PM}}^{\text{CH}} - \gamma_{\text{PM}}^{\text{NH}} = \phi_{\text{H}}$ , while  $\beta_{\text{PM}}^{\text{CH}}$  and  $\beta_{\text{PM}}^{\text{NH}}$  are related to the bond angles.

It is perhaps worth mentioning that the torsion angle  $\phi$  is manifest in the dipolar spectrum whether or not both double- and zero-quantum coherences are involved. In the  $\text{H--C=C--H}$  experiment,<sup>13</sup> for example, only the C–C double-quantum coherence is excited. In general, as long as a correlated spin state between the  $^{15}\text{N}$  and the  $^{13}\text{C}$  spins is created, the geometric relation between the N–H and C–H dipolar tensor orientations can be probed spectroscopically. The presence of both the sum and the difference dipolar phases in eq 4 results from the symmetry of the dipolar interactions, not from the coexistence of the double- and zero-quantum coherences.

#### 4. Numerical Simulations

The indirectly detected N–C multiple-quantum dipolar sideband spectrum is simulated by evaluating eq 4 over the course of the evolution period  $t_1$ . Powder averaging was performed by Monte Carlo integration where the Euler angles  $\Omega_{\text{MR}}$  that transform the molecular frame to the rotor frame are randomly generated according to a powder distribution. The time signals due to HMQ evolution are coadded and normalized by the number of crystallites. Input parameters for the simulation comprise the effective dipolar couplings  $\kappa\delta_{\text{CH}}$  and  $\kappa\delta_{\text{NH}}$ , which are obtained from the  $^{15}\text{N}$  and  $^{13}\text{C}$  DIPSHIFT experiments described below, the Euler angles  $\Omega_{\text{PM}}$  and  $\Omega_{\text{MR}}$ , the mixing time  $\tau$  for the double- and zero-quantum coherences, the spinning speed  $\omega_r$ , the spectral width, and the number of crystallites employed in the powder average.

#### 5. One-Bond N–H and C–H Dipolar Couplings

The simulation of the  $\phi$ -dependent dipolar sideband spectrum requires  $\text{C}^\alpha\text{--H}^\alpha$  and  $\text{N--H}^{\text{NH}}$  dipolar couplings as input parameters. Thus, the magnitudes of these couplings affect the accuracy of the  $\phi$  measurement. The effective heteronuclear

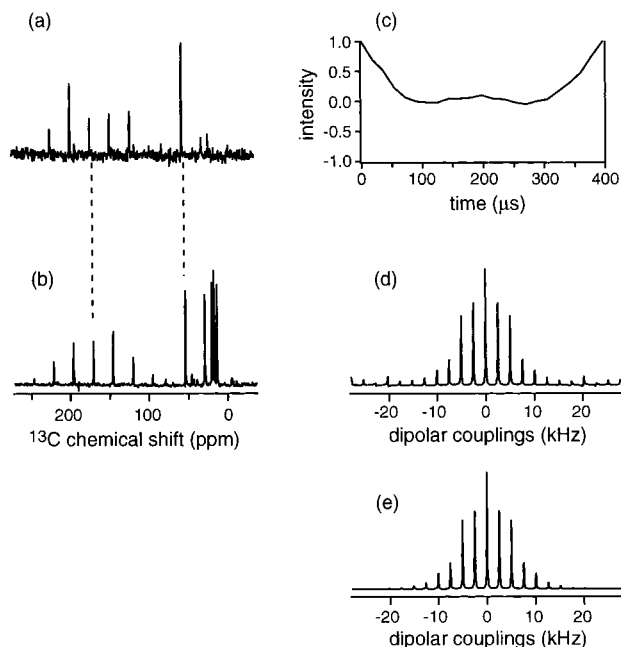


**Figure 4.**  $^{15}\text{N}$ – $^{13}\text{C}$  HMQ spectrum of NAV for determining the torsion angle  $\phi_{\text{H}}$ , acquired at  $\omega_r/2\pi = 2525$  Hz. (a)  $^{13}\text{C}$  MAS spectrum obtained with HMQ excitation and reconversion, but zero evolution time. 512 scans were added. The HMQ filter selects only the  $\text{C}^\alpha$  and the acetyl carbonyl resonances, which are directly bonded to the  $^{15}\text{N}$  atom. (b)  $^{13}\text{C}$  CPMAS spectrum of NAV after 256 scans, exhibiting all  $^{13}\text{C}$  chemical shift resonances. (c) Time evolution of the N– $\text{C}^\alpha$  double- and zero-quantum coherences under the C–H and N–H dipolar couplings for one rotor period. The intensity unit is arbitrary. (d) Projected HMQ dipolar sideband spectrum of the  $\text{C}^\alpha$  resonance, in which the highest intensity is observed at the centerband. (e) Best-fit simulation of the  $\text{C}^\alpha$  spectrum, obtained with  $\phi_{\text{H}} = 165^\circ$ . Other input parameters are  $\kappa\delta_{\text{CH}} = 10.9$  kHz,  $\kappa\delta_{\text{NH}} = -5.2$  kHz,  $\omega_r/2\pi = 2525$  Hz,  $\beta_{\text{PM}}^{\text{CH}} = 109.5^\circ$ ,  $\beta_{\text{PM}}^{\text{NH}} = 60^\circ$ ,  $\gamma_{\text{PM}}^{\text{CH}} = 0^\circ$ ,  $\gamma_{\text{PM}}^{\text{NH}} = 165^\circ$ ,  $\tau = 792$   $\mu\text{s}$ , and 5000 crystallite orientations.

couplings in our experiments are the product of the rigid-limit anisotropies  $\delta_\lambda$  and the scaling factor  $\kappa$  of the homonuclear decoupling sequence. Theoretically,  $\kappa = 0.536$  for semiwindowless MREV-8.<sup>28</sup> However, the actual  $\kappa$  value usually deviates from theory due to experimental imperfections and is best obtained empirically under the same conditions as the torsion angle experiment. We determined the N– $\text{H}^{\text{N}}$  and  $\text{C}^\alpha$ – $\text{H}^\alpha$  couplings by a 2D MAS separated-local-field technique that separates dipolar rotational sideband patterns according to the isotropic chemical shifts of the  $^{15}\text{N}$  or  $^{13}\text{C}$  sites (DIPSHIFT).<sup>29–31</sup> The resulting rotational sideband patterns in  $\omega_1$  are then simulated to yield the coupling strengths. As indicated in Figure 3b, these DIPSHIFT experiments are executed in a constant-time fashion with a  $180^\circ$  refocusing pulse in order to be comparable to the torsion angle measurement. Since the performance of the multiple-pulse sequence that determines the scaling factor  $\kappa$  depends on the ratio of the multiple-pulse cycle time ( $\tau_c$ ) to the rotor period ( $\tau_r$ ), the MREV-8 pulse length and the spinning speeds in the DIPSHIFT experiments were kept similar to those used in the torsion angle measurement.

## 6. Results and Discussion

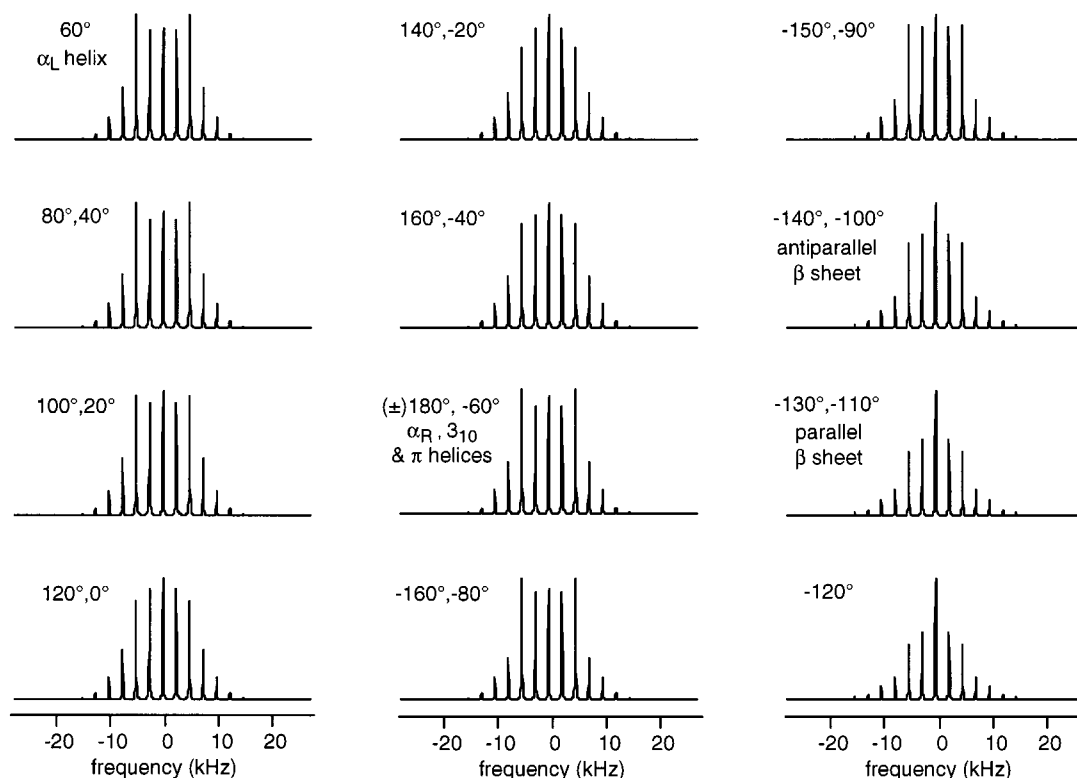
Figure 4a is the  $\omega_2$  projection of the 2D N–C multiple-quantum spectrum of NAV. Compared to the  $^{13}\text{C}$  CPMAS spectrum (Figure 4b), only the  $\text{C}^\alpha$  and the acetyl carbonyl resonances are observed, while other  $^{13}\text{C}$  signals are efficiently suppressed by the short excitation time of the HMQ filter. The signal-to-noise ratios of the two spectra indicate that the HMQ excitation efficiency is approximately 36%.

The  $t_1$  modulation of the  $\text{C}^\alpha$  peak is shown in Figure 4c. The net signal decay after one rotor cycle (396  $\mu\text{s}$ ) is negligible: in general, we found that more than 80% of the initial signal intensity could be reproducibly refocused at the rotor echo. The time signal is quite symmetric with respect to the center of the rotor period, as expected for an inhomogeneous spin system evolving under MAS.<sup>32</sup> The high echo intensity and the symmetry demonstrate the excellent performance of the homonuclear decoupling sequence, since under ideal multiple-pulse decoupling, any intensity loss must result from true  $T_2$  relaxation, which is not expected to be significant after about 400  $\mu\text{s}$  (the  $^1\text{H}$  homogeneous line width is likely to be smaller than 2.5 kHz). In our experiments, the MREV-8 performance is ensured by the short cycle time relative to the rotor period ( $\tau_c = \tau_r/12$ ), since this minimizes undesirable interference effects between sample spinning and multiple-pulse decoupling.<sup>33</sup>

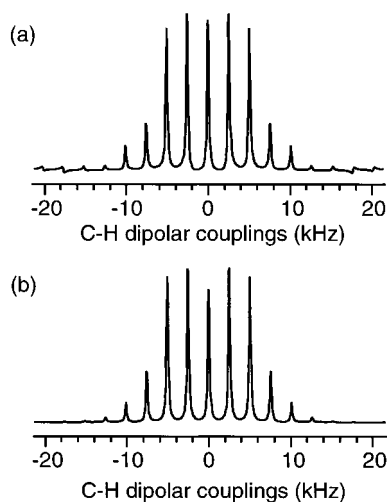
In order to obtain  $\phi$ -dependent spectra in the form of rotational sideband patterns, the  $t_1$  modulation must be periodic. This was achieved by equalizing the echo intensity to the initial intensity (of the first  $t_1$  point) by positive exponential multiplication  $\exp(+t_1/T_2)$ , then replicating the single- $\tau_r$  signal several times, followed by a negative exponential multiplication  $\exp(-t_1/T_2)$  to restore the original decay.<sup>31,34</sup> Assuming equal line widths for all dipolar sidebands, the periodicity of the MAS time signal dictates that the  $\phi$ -dependent sideband pattern obtained in this way is the same as obtained by acquiring the complete  $t_1$  signal over many rotor cycles.

Figure 4d shows the projection of the N–C multiple-quantum sideband spectrum of the  $\text{C}^\alpha$  resonance. From 2D  $^{13}\text{C}$  DIPSHIFT experiments, we found that a single  $\omega_1$  cross section at the maximum intensity of the  $\text{C}^\alpha$  resonance produces slightly inaccurate sideband intensities as a result of inhomogeneous broadening of the  $\text{C}^\alpha$  peak in the  $\omega_2$  dimension. Therefore,  $\omega_1$  slices across the  $\text{C}^\alpha$  resonance line width were summed and used for extracting the angle  $\phi$ . The projected spectrum is characterized by a high centerband intensity and lower but significant intensities up to the fourth order sidebands, with observable noise extending to the two edges of the spectral window. The spectrum is simulated with  $|\phi_{\text{H}}| = 165^\circ$  (Figure 4e), which corresponds to a backbone torsion angle  $\phi = -135^\circ$  or  $-105^\circ$  for the L-isomer. The first angle agrees remarkably well with the X-ray crystal structure (Figure 2), in which C(O)–N– $\text{C}^\alpha$ –C(O) was determined to be  $-136.5^\circ$ .<sup>35</sup> The presence of two possible  $\phi$  angles results from the invariance of the spectra to the sign of  $\phi_{\text{H}}$ . Such degeneracies also arise when distances are employed as a means to determine torsion angles that characterize secondary structures.<sup>36</sup>

To demonstrate the resolution of the angle  $\phi$  measured by the HMQ technique, we show simulated N–C HMQ spectra as a function of  $\phi$  in Figure 5. Since  $\pm\phi_{\text{H}}$  yield the same dipolar sideband spectra, and  $\phi_{\text{H}} = \phi - 60^\circ$  for L-amino acids, each simulated spectrum corresponds to two  $\phi$  angles ( $\phi_1, \phi_2$ ) related by  $(\phi_1 + \phi_2)/2 = -120^\circ$ . Figure 5 indicates that the sideband patterns change more drastically when the N– $\text{H}^{\text{N}}$  and  $\text{C}^\alpha$ – $\text{H}^\alpha$  bonds are antiparallel ( $\phi_{\text{H}} = 180^\circ$  or  $\phi = -120^\circ$ ) than when they are parallel ( $\phi_{\text{H}} = 0^\circ$  or  $\phi = 60^\circ$ ). By simple inspection, the angular resolution is estimated to be less than  $\pm 10^\circ$  for the former and  $\pm 20^\circ$  for the latter. Typical protein secondary structures with their corresponding values of  $\phi$  are also indicated in Figure 5. It can be seen that the spectra of helical structures ( $\alpha$ ,  $3_{10}$ , and  $\pi$  helices) are clearly different from those of  $\beta$  sheets. It should be emphasized that these dipolar sideband patterns are dominated by the angle  $\phi$  and much less affected by other parameters such as the effective C–H and N–H dipolar couplings.



**Figure 5.** Simulation of N–C multiple-quantum dipolar sideband spectra as a function of  $\phi$ . Each spectrum corresponds to two  $\phi$  angles due to the spectral invariance to  $\pm\phi_H$ . Only the L-configuration of  $C^\alpha$  is considered. The spectra are unique in the range  $\phi = [60, -120^\circ]$  and have the highest angular resolution around  $\phi = -120^\circ$ . Spectra simulated with angles  $\phi$  that correspond to typical protein secondary structures are labeled accordingly. Input parameters for the simulation are  $\kappa\delta_{CH} = 10.9$  kHz,  $\kappa\delta_{NH} = -5.2$  kHz,  $\tau = 792$   $\mu$ s,  $\omega_r/2\pi = 2525$  Hz,  $\beta_{PM}^{CH} = 109.5^\circ$ ,  $\beta_{PM}^{NH} = 60^\circ$ ,  $\gamma_{PM}^{CH} = 0^\circ$ ,  $\gamma_{PM}^{NH} = \phi_H$ , and 5000 crystallite orientations.



**Figure 6.** (a) NAV  $C^\alpha$ –H dipolar sideband pattern from a 2D  $^{13}\text{C}$  DIPSHIFT experiment at  $\omega_r/2\pi = 2525$  Hz.  $\omega_1$  slices within the  $C^\alpha$  resonance line width were summed to compensate for inhomogeneous broadening. (b) Best-fit simulation, with a  $C^\alpha$ – $H^\alpha$  coupling of 10.9 kHz. Two smaller couplings of 1.4 kHz approximating the effects of long-range  $C^\alpha$ – $H^N$  and  $C^\alpha$ – $H^\beta$  couplings were also used in the simulation.

The  $C^\alpha$ – $H^\alpha$  and N– $H^N$  couplings used in the simulation of the  $\phi$ -dependent spectra were determined by  $^{13}\text{C}$  and  $^{15}\text{N}$  DIPSHIFT experiments conducted with the pulse sequence of Figure 3b. The resulting  $C^\alpha$ –H dipolar sideband spectrum can be simulated with an effective  $C^\alpha$ – $H^\alpha$  coupling of 10.9 kHz, as shown in Figure 6. This coupling strength is about 10% smaller than expected for a 1.1 Å C–H bond ( $\delta_{CH} = -22.7$  kHz) under a semiwindowless MREV-8 sequence ( $\kappa = 0.536$ ). Such a reduction of one-bond C–H couplings in rigid solids has been previously observed and discussed extensively.<sup>31,37–39</sup>

It may be attributed to several factors, such as high-frequency vibrations of the internuclear bond, imperfect homonuclear decoupling, and long-range C–H dipolar couplings. In our experiment, since the deviation of the effective coupling from the expected value is relatively small, we did not investigate the exact causes of the difference. In the simulation of the  $^{13}\text{C}$  DIPSHIFT spectrum, we considered not only the directly bonded  $C^\alpha$ – $H^\alpha$  coupling, but also long-range  $C^\alpha$ – $H^\beta$  and  $C^\alpha$ – $H^N$  couplings, which were necessary for reproducing the centerband intensity of the experimental spectrum. Although these long-range couplings also contain information on torsion angles, namely, the angle  $H^\alpha$ – $C^\alpha$ – $C^\beta$ – $H^\beta$  (from the  $C^\alpha$ – $H^\beta$  coupling) and  $\phi_H$  (from the  $C^\alpha$ – $H^N$  coupling), they do not affect the line shape of the torsion angle spectra considerably and thus were not employed in the simulations of the  $\phi$ -dependent HMQ spectra (Figures 3 and 5). For the DIPSHIFT simulation, angles estimated from the X-ray structure of NAV were used as  $\Omega_{PM}$  that describe the orientations of the  $C^\alpha$ – $H^\beta$  and  $C^\alpha$ – $H^N$  dipolar coupling tensors in the molecular frame.

In the  $^{15}\text{N}$  2D DIPSHIFT spectrum,  $^{15}\text{N}$  chemical shift sidebands were observed in the  $\omega_2$  dimension (Figure 7a) due to the large  $^{15}\text{N}$  chemical shift anisotropy relative to the spinning speed. Thus, the N– $H^N$  dipolar coupling spectrum (Figure 7b) was obtained by integrating the  $\omega_1$  cross sections at these sideband frequencies. Simulation of the projected dipolar spectrum yields an effective N– $H^N$  coupling of  $-5.2$  kHz (Figure 7c), which corresponds to a MREV-8 scaling factor of 0.48 if a N–H bond length of 1.049 Å is used.<sup>39</sup> The reduction in  $\kappa$  is similar to that observed in the  $^{13}\text{C}$  DIPSHIFT experiment. No long-range N–H couplings were used in the simulation.

## 7. Conclusions

We described the determination of the torsion angle  $\phi$  in solid peptides by a 2D MAS technique utilizing  $^{15}\text{N}$ – $^{13}\text{C}$  double-

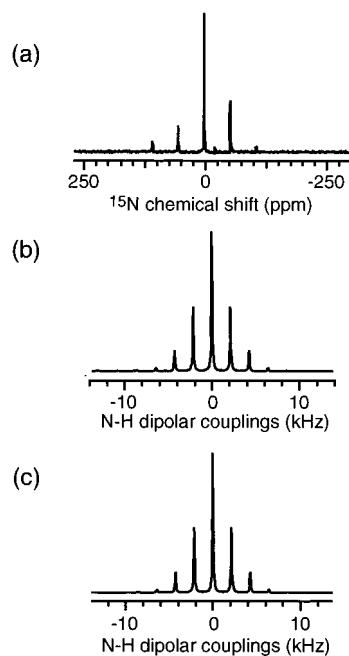


**Figure 7.** (a) NAV  $^{15}\text{N}$  CPMAS spectrum, taken from the  $\omega_2$  projection of a 2D  $^{15}\text{N}$  DIPSHIFT spectrum acquired at  $\omega_1/2\pi = 2137$  Hz. (b) N-H dipolar sideband spectrum, obtained by summing up the  $\omega_1$  cross sections at the  $^{15}\text{N}$  chemical shift sidebands. (c) Simulation with a N-H $^{\text{N}}$  coupling of  $-5.2$  kHz, and without long-range couplings.

and zero-quantum coherences. The angle  $\phi$  is obtained from the relative orientations of the N-H $^{\text{N}}$  and C $^{\alpha}$ -H $^{\alpha}$  bonds, which are reflected in the sideband spectrum of the sum and difference of the C $^{\alpha}$ -H $^{\alpha}$  and N-H $^{\text{N}}$  dipolar couplings. The N-C dipolar interaction is recoupled by rotor-synchronized  $180^\circ$  pulses, and the multiple-quantum coherences can be excited with an efficiency of about 36% under optimum conditions. Applied to NAV, the experiment yielded an angle  $\phi$  of  $-135^\circ$  or  $-105^\circ$ , the first of which agrees well with the X-ray crystal structure. Simulation indicates that this technique has an angular resolution of less than  $10^\circ$  when the N-H $^{\text{N}}$  and C $^{\alpha}$ -H $^{\alpha}$  bonds are nearly antiparallel and  $20^\circ$  when they are nearly parallel. The accuracy of the experiment is improved by determining the effective C $^{\alpha}$ -H $^{\alpha}$  and N-H $^{\text{N}}$  couplings with control DIPSHIFT experiments. These dipolar couplings not only serve as reliable input parameters for simulating the torsion angle spectrum but also check the performance of the homonuclear decoupling sequence.

Since the  $\phi$ -dependent sideband patterns are separated according to the  $^{13}\text{C}$  isotropic chemical shifts, the technique allows the extraction of  $\phi$  angles in various residues simultaneously, as long as the C $^{\alpha}$  isotropic shifts are resolved. This represents the first solid-state NMR technique that can provide quantitative structural information on multiple sites in a polypeptide. In terms of sensitivity of the technique, we estimate that sufficiently sensitive spectra can be obtained in 24 h on 60 mg of a 100%  $^{15}\text{N}$ -labeled peptide with repeat units of six residues. Alternatively, larger proteins of up to 15 kDa can be characterized in about 3 days if 100% enrichment in  $^{15}\text{N}$  and  $\sim 20\%$  in  $^{13}\text{C}$  are provided. The multiple-quantum nature of the technique is expected to alleviate the problem of multispin couplings, which are encountered in distance measurements of highly labeled systems, so that  $\phi$  angles in uniformly and fractionally  $^{15}\text{N}$  and  $^{13}\text{C}$  labeled samples can be determined. Finally, the angular resolution of the technique can be further enhanced by increasing the spectral variation with  $\phi$  through the adjustment of the C-H and N-H coupling strengths. Combined with techniques that

measure peptide  $\psi$  angles,<sup>14</sup> this should allow the distinction between similar secondary structures such as the  $\alpha$  helix and the  $3_{10}$  helix, or the antiparallel and the parallel  $\beta$  sheets. Efforts in these directions are currently pursued in this laboratory.

**Acknowledgment.** We would like to thank Chad Rienstra for building the triple-resonance transmission-line probe. M.H. thanks Prof. Klaus Schmidt-Rohr for many helpful discussions on double-quantum spectroscopy. This research was supported by the National Institutes of Health (GM-23403, GM-23289, and RR-00995).

## References and Notes

- (1) Raleigh, D. P.; Levitt, M. H.; Griffin, R. G. *Chem. Phys. Lett.* **1988**, *146*, 71.
- (2) Levitt, M. H.; Raleigh, D. P.; Creuzet, F.; Griffin, R. G. *J. Chem. Phys.* **1990**, *92*, 6347.
- (3) Tycko, R.; Dabbagh, G. *Chem. Phys. Lett.* **1990**, *173*, 461.
- (4) Bennett, A. E.; Ok, J. H.; Griffin, R. G.; Vega, S. *J. Chem. Phys.* **1992**, *96*, 8624.
- (5) Sun, B.-Q.; Costa, P. R.; Kocisko, D.; Lansbury, P. T. J.; Griffin, R. G. *J. Chem. Phys.* **1995**, *102*, 702.
- (6) Gullion, T.; Schaefer, J. *J. Magn. Reson.* **1989**, *81*, 196.
- (7) Oas, T. G.; Griffin, R. G.; Levitt, M. H. *J. Chem. Phys.* **1988**, *89*, 692.
- (8) Levitt, M. H.; Oas, T. G.; Griffin, R. G. *Isr. J. Chem.* **1988**, *28*, 271.
- (9) Costa, P. R.; Sun, B. Q.; Griffin, R. G. Manuscript in preparation.
- (10) Creighton, T. E. *Proteins: Structures and Molecular Properties*, 2nd ed.; W. H. Freeman and Co.: New York, 1993.
- (11) Karplus, M. *J. Chem. Phys.* **1959**, *30*, 11.
- (12) Wang, A. C.; Bax, A. *J. Am. Chem. Soc.* **1996**, *118*, 2483.
- (13) Feng, X.; Lee, Y. K.; Sandstroem, D.; Eden, M.; Maisel, H.; Sebald, A.; Levitt, M. H. *Chem. Phys. Lett.* **1996**, *257*, 314.
- (14) Schmidt-Rohr, K. *J. Am. Chem. Soc.* **1996**, *118*, 7601.
- (15) Mehta, M. A.; Bower, P.; Gregory, D.; Zebroski, H.; Drobny, G. *37th Experimental NMR Conference*, Asilomar, CA, 1996.
- (16) Gregory, D.; Mehta, M. A.; Drobny, G. *37th Experimental NMR Conference*, Asilomar, CA, 1996.
- (17) Weliky, D.; Tycko, R. *J. Am. Chem. Soc.* **1996**, *118*, 8487.
- (18) Ishii, Y.; Terao, T.; Kainosho, M. *Chem. Phys. Lett.* **1996**, *256*, 133.
- (19) Mueller, L. *J. Am. Chem. Soc.* **1979**, *101*, 4481.
- (20) Minoretto, A.; Aue, W. P.; Reinhold, M.; Ernst, R. R. *J. Magn. Reson.* **1980**, *40*, 175.
- (21) Bax, A.; Griffey, R. H.; Hawkins, B. L. *J. Magn. Reson.* **1983**, *55*, 301.
- (22) Pan, Y.; Gullion, T.; Schaefer, J. *J. Magn. Reson.* **1990**, *90*, 330.
- (23) Christensen, A. M.; Schaefer, J. *Biochemistry* **1993**, *32*, 2868.
- (24) Gullion, T.; Schaefer, J. In *Advances in Magnetic Resonance*; Warren, W. S., Ed.; Academic Press: San Diego, 1989; p 57.
- (25) Bennett, A. E.; Griffin, R. G.; Vega, S. In *NMR Basic Principles and Progress*; Diehl, P., Fluck, E., Kosfeld, E., Eds.; Springer: Berlin, 1994; p 1.
- (26) Shirley, J. M. *Phys. Rev. B* **1965**, *138*, 979.
- (27) Spiess, H. W. In *NMR Basic Principles and Progress*; Diehl, P., Fluck, E., Kosfeld, E., Eds.; Springer: Berlin, 1978.
- (28) Rhim, W.-K.; Elleman, D. D.; Vaughan, R. W. *J. Chem. Phys.* **1973**, *59*, 1740.
- (29) Munowitz, M. G.; Griffin, R. G.; Bodenhausen, G.; Huang, T. H. *J. Am. Chem. Soc.* **1981**, *103*, 2529.
- (30) Munowitz, M.; Aue, W. P.; Griffin, R. G. *J. Chem. Phys.* **1982**, *77*, 1686.
- (31) Schaefer, J.; McKay, R. A.; Stejskal, E. O. *J. Magn. Reson.* **1983**, *52*, 123.
- (32) Maricq, M. M.; Waugh, J. S. *J. Chem. Phys.* **1979**, *70*, 3300.
- (33) Haeblerlen, U.; Waugh, J. S. *Phys. Rev.* **1968**, *175*, 453.
- (34) Schaefer, J.; Stejskal, E. O.; McKay, R. A.; Dixon, W. T. *Macromolecules* **1984**, *17*, 1479.
- (35) Carroll, P. J.; Stewart, P. L.; Opella, S. J. *Acta Crystallogr.* **1990**, *C46*, 243.
- (36) Spencer, R. G. S.; Halverson, K. J.; Auger, M.; McDermott, A. E.; Griffin, R. G.; Lansbury, P. T. *Biochemistry* **1991**, *30*, 10382.
- (37) Schaefer, J.; Stejskal, E. O.; McKay, R. A. *J. Magn. Reson.* **1984**, *57*, 85.
- (38) Webb, G. G.; Zilm, K. W. *J. Am. Chem. Soc.* **1989**, *111*, 2455.
- (39) Roberts, J. E.; Harbison, G. S.; Munowitz, M. G.; Herzfeld, J.; Griffin, R. G. *J. Am. Chem. Soc.* **1987**, *109*, 4163.